THE PROTEIN SOCIETY

Ca^{2+} and Mg^{2+} modulate conformational dynamics and stability of downstream regulatory element antagonist modulator

Khoa Pham,[1] Gangadhar Dhulipala,[1] Walter G. Gonzalez,[1] Bernard S. Gerstman,[2] Chola Regmi,[2] Prem P. Chapagain,[2] and Jaroslava Miksovska[1]*

[1]Department of Chemistry and Biochemistry, Florida International University, Miami, Florida 33199
[2]Department of Physics, Florida International University, Miami, Florida 33199

Received 4 September 2014; Accepted 25 January 2015
DOI: 10.1002/pro.2646
Published online 27 January 2015 proteinscience.org

Abstract: Downstream Regulatory Element Antagonist Modulator (DREAM) belongs to the family of neuronal calcium sensors (NCS) that transduce the intracellular changes in Ca^{2+} concentration into a variety of responses including gene expression, regulation of Kv channel activity, and calcium homeostasis. Despite the significant sequence and structural similarities with other NCS members, DREAM shows several features unique among NCS such as formation of a tetramer in the apo-state, and interactions with various intracellular biomacromolecules including DNA, presenilin, Kv channels, and calmodulin. Here we use spectroscopic techniques in combination with molecular dynamics simulation to study conformational changes induced by Ca^{2+}/Mg^{2+} association to DREAM. Our data indicate a minor impact of Ca^{2+} association on the overall structure of the N- and C-terminal domains, although Ca^{2+} binding decreases the conformational heterogeneity as evident from the decrease in the fluorescence lifetime distribution in the Ca^{2+} bound forms of the protein. Time-resolved fluorescence data indicate that Ca^{2+}binding triggers a conformational transition that is characterized by more efficient quenching of Trp residue. The unfolding of DREAM occurs through an partially unfolded intermediate that is stabilized by Ca^{2+} association to EF-hand 3 and EF-hand 4. The native state is stabilized with respect to the partially unfolded state only in the presence of both Ca^{2+} and Mg^{2+} suggesting that, under physiological conditions, Ca^{2+} free DREAM exhibits a high conformational flexibility that may facilitate its physiological functions.

Keywords: DREAM; potassium channel interacting protein; EF-hand motif; neuronal calcium sensors; tryptophan emission; equilibrium unfolding

Introduction

EF-hand motif Ca^{2+} binding proteins are involved in the regulation of numerous intracellular processes ranging from gene expression, cell division, cell growth, as well as apoptosis. All members of this family carry at least one pair of EF-hand calcium binding sites that bind calcium with equilibrium affinity constants ranging from 10^4M in the case of S100 proteins, to 10^8M as found for parvalbumin.[1] The protein affinity for Ca^{2+} is fine-tuned by the amino acid sequence of the EF-hand binding site, overall structure of the Ca^{2+} sensor, and by interactions with

Abbreviations: DREAM, downstream regulatory element antagonist modulator; NCS, neuronal calcium sensor.

Grant sponsor: National Science Foundation; Grant number: MCB 1021831 (to J.M.); Grant sponsor: James & Esther King Biomedical Research Program, Florida Department of Health (to J.M.).

Gangadhar Dhulipala's current address is Regeneron Pharmaceuticals Inc., 777 Old Saw Mill River Rd, Tarrytown, NY 10601.

*Correspondence to: Jaroslava Miksovska, Department of Chemistry and Biochemistry, Florida International University, 11200 SW 8th Street, Miami, FL 33199.
E-mail: miksovsk@fiu.edu

other intracellular partners. Despite relatively high sequence similarities, EF-hand proteins exhibit large structural diversity in the apo- and Ca^{2+} bound forms that is essential for specific interactions with intracellular partners and functional diversity.[2]

For example, in calmodulin and troponin C, two independent domains are connected by a flexible α-helical linker and calcium association leads to a substantial reorganization of the C- and N-terminal domains and exposure of hydrophobic patches on the protein surface. In calmodulin, such highly dynamic protein structure enables specific interactions with a large number of intracellular targets.[2] Unlike the calmodulin family, structural changes linked to Ca^{2+} binding to EF-hands in S100 proteins are relatively modest and result in exposure of a wider and flatter hydrophobic crevice on the protein surface that facilitates binding of intracellular partners.[3] On the other hand, in neuronal calcium sensors (NCS), the calcium association leads to the structural reorganization that promotes repositioning of the N- and C-terminal domain and in some proteins exposure of the myristoyl group.

NCS are predominantly expressed in neuronal tissue where they regulate numerous intracellular processes including vision transduction, potassium voltage channel kinetics, DNA expression, etc.[4–6] All members carry four EF-hand binding sites, although only two or three EF-hands are active and bind bivalent ions with a high affinity.[5] Some members of the NCS family undergo post-translational modifications such as fatty acid esterification at the N-terminus. The presence of the fatty acid modulates the range of Ca^{2+} triggered conformational switching and facilitates protein association to the membrane.[7] The C- and N-terminal domains in NCS are each organized in a globular arrangement and are connected by a short U-shaped linker with a solvent-exposed hydrophobic groove stretching between the C- and N-terminal domains.[8]

DREAM, also known as KChIP3 or calsenilin, belongs to the subfamily of NCS potassium channel interacting proteins (KChIP), which includes three additional members (KChIP1, KChIP2, and KChIP4).[9] All members share a conserved region of 180 residues along with highly variable N-termini of 35 to 100 residues.[10] In DREAM, EF-hand 1 has no function due to the presence of Cys104 and Pro105 prevent this site from binding to Ca^{2+}/Mg^{2+}, whereas the canonical EF-hand 3 and EF-hand 4 functionally bind Ca^{2+} with a high affinity (K_d ~1–10 μ*M*) and EF-hand 2 structurally binds Mg^{2+} (K_d ~14 μ*M*).[26] KChIP1, DREAM, and KChIP4 are predominantly expressed in the brain where they regulate gating properties of Kv channels and the surface expression of the Kv4 complex.[11,12] Unlike other members of the KChIP subfamily, DREAM interacts with numerous intracellular partners including calmodulin,[13] DNA,[14] presenilin,[15–19] and CREB/CREM transcription factors.[20,21]

The role of Ca^{2+} in regulating DREAM functions and the structural basis of DREAM interactions with multiple partners are not fully understood. Although the solution structure of Ca^{2+} bound DREAM (residues 76–256) is known[22] as well as the solution structure of the C-terminal domain (residues 161–256) of Ca^{2+} bound DREAM,[23] it is unclear how the Ca^{2+}/Mg^{2+} association to the EF hands alters the structural properties of DREAM. Considering the large number of DREAM interacting proteins, understanding the structural diversity could provide important insight into the relationship between the sequence, structure, and the target diversity of DREAM and NCS proteins in general. Since the single tryptophan (Trp169) is located between the N- and C-terminal domain in DREAM (Fig. 8), this residue is ideal for monitoring conformational response to changes in Ca^{2+}/Mg^{2+} concentration. Thus we have combined time-resolved fluorescence, CD spectroscopy, and molecular dynamics to probe the dynamics and structural diversity of DREAM under various conditions. The heterogeneous Trp emission decay indicates that DREAM adopts multiple conformations in the apo and Ca^{2+} bound forms. Ca^{2+} binding to EF-hands is associated with increased protein rigidity and a decrease in Trp solvent exposure. DREAM unfolds through a partially unfolded intermediate state that is populated at a GuHCl concentration around 4.5 to 5.0*M*. The intermediate state is stabilized by Ca^{2+} binding to EF-hand 3 and EF-hand 4. The presence of Mg^{2+} stabilizes the native structure of Ca^{2+} bound DREAM with respect to the intermediate state.

Results

Steady-state emission spectra

The emission spectra of apoDREAM and Mg^{2+}DREAM are almost identical, and are broad with a maximum at 340 nm (Fig. 1). Upon Ca^{2+} association to DREAM or Mg^{2+}DREAM, we observed that the two spectra change in the same manner with a decrease in the emission intensity along with a concomitant hypsochromic shift of 5 nm. Analogous Ca^{2+} triggered bathochromic shifts were reported previously, although the emission spectra presented here are approximately 5 nm blue shifted compared with the published results.[24] The protein was purified and studied in the presence of LDAO since the previous study had shown that the addition of LDAO reduces protein aggregation and stabilizes apoDREAM and Ca^{2+}DREAM in its tetrameric and dimeric form, respectively.[24] We have observed that the presence of LDAO strongly impacts the emission spectra of Ca^{2+} free and Ca^{2+} bound DREAM. For example, DREAM samples dialyzed against 20 m*M* Tris buffer, 1 m*M* DTT, and 10 m*M* LDAO at pH 7.4 for 48 h provided emission spectra

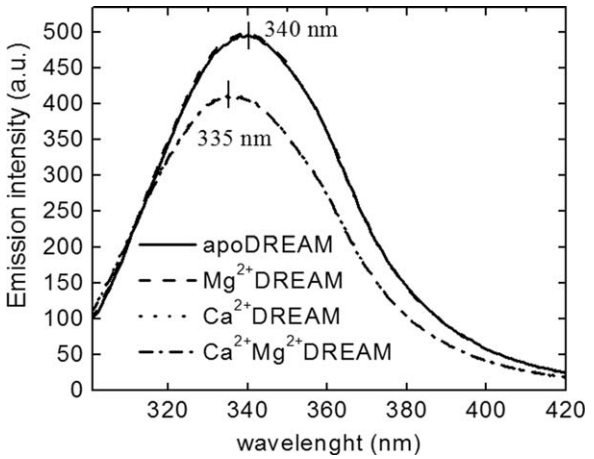

Figure 1. Fluorescence emission spectra of apo-, Mg^{2+}, Ca^{2+}, and $Ca^{2+}Mg^{2+}$DREAM upon excitation at 295 nm. Note that the emission spectrum of apoDREAM and Mg^{2+}DREAM are almost identical, and likewise for Ca^{2+}DREAM and $Ca^{2+}Mg^{2+}$DREAM.

with a λ_{max} of 340 nm and 335 nm for apo- and Ca^{2+}DREAM, respectively, which are comparable to those reported by Osawa *et al.*[24] On the other hand, emission spectra of DREAM samples prepared in the absence of LDAO are blue shifted with an emission maximum at ~330 nm for Ca^{2+}DREAM and 335 nm for apoDREAM suggesting that LDAO binding to DREAM increases the solvent exposure of the Trp side-chain. The fluorescence quantum yield was determined to be 0.105 ± 0.009 for apo- and Mg^{2+}DREAM and 0.090 ± 0.011 in Ca^{2+} and $Ca^{2+}Mg^{2+}$DREAM. The bathochromic shift of the Trp emission maximum suggest that Ca^{2+} association to DREAM leads to a conformational transition upon which the Trp residue moves towards the hydrophobic core of the protein.

Fluorescence quenching

Acrylamide, a polar, uncharged water soluble molecule, was used in quenching studies to further probe the solvent accessibility of Trp169 in DREAM. The plot of the ratio of the DREAM fluorescence emission intensities in the absence and presence of the acrylamide quencher exhibit a linear dependence (Fig. 2) with Stern-Volmer constants [Eq. (1)] of $2.80 \pm 0.01M^{-1}$ for apoDREAM and $2.03 \pm 0.10M^{-1}$ for Ca^{2+}DREAM, and $1.78 \pm 0.01M^{-1}$ for $Ca^{2+}Mg^{2+}$DREAM confirming that the Trp169 side-chain is less solvent accessible in the structure of Ca^{2+} bound DREAM. In the case of collisional quenching, the bimolecular quenching rate constant, $k_q = K_{SV}/<\tau>$, where $<\tau>$ is the lifetime in the absence of the quencher, provides a better estimate of the quenching efficiency. Using the average value for the fluorescence lifetime (Table I), the k_q value was determined to be 6.2 x $10^8 M^{-1}$ s^{-1} for apoDREAM and 4.2 x $10^8 M^{-1}$ s^{-1} for Ca^{2+}DREAM, and 3.7 x $10^8 M^{-1}$ s^{-1} for $Ca^{2+}Mg^{2+}$DREAM. Interestingly, Mg^{2+} association to DREAM results in a small but reproducible decrease in the Stern-Volmer constant and the bimolecular quenching constant, $K_{sv} = 2.29 \pm 0.06M^{-1}$ and $k_q = 5.0$ x $10^8 M^{-1}$ s^{-1}, indicating that Mg^{2+} binding to EF-hand 2 causes a minor structural reorganization that impacts the Trp169 solvent accessibility. Previously, we have shown that Mg^{2+} binding to DREAM leads to small changes in the fluorescence properties of 1,8-ANS DREAM complexes,[25] supporting the role of Mg^{2+} in stabilizing the tertiary structure of the DREAM protein.

Fluorescence lifetime

Since the Trp fluorescence lifetime is highly sensitive to small variations in the fluorophore environment, probing the lifetime of the single Trp residue (Trp169) provides further insight into Mg^{2+}/Ca^{2+} induced conformational changes, including alteration of local dynamics. The Trp169 lifetime was determined using phase modulation fluorescence spectroscopy. The phase shift and modulation ratio data were monitored in the frequency range from 5 MHz to 250 MHz and are presented in Figure 3. Data were analyzed using either a sum of discrete exponentials or various distribution models (Gaussian, Lorentzian or uniform). The best fits based on residuals and χ^2 values were obtained with a model composed of a discrete single exponential decay component and a continuous Gaussian distribution (Table I). The discrete component exhibits a calcium independent lifetime of ~7.5 ns whereas the Gaussian distribution is centered at 3.5 ns and 1.7 ns for Ca^{2+} free and Ca^{2+} bound DREAM, respectively. The width of the distribution is $w_1 = 1.8$ ns and 2.0 ns in the apo-DREAM and Mg^{2+}DREAM, respectively, and narrows upon Ca^{2+} binding to $w_1 = 0.8$ ns and 0.9 ns in Ca^{2+}DREAM and $Ca^{2+}Mg^{2+}$DREAM, respectively. In addition, the fractional contribution of the 7.5 ns component is ~0.12 in the apo- and

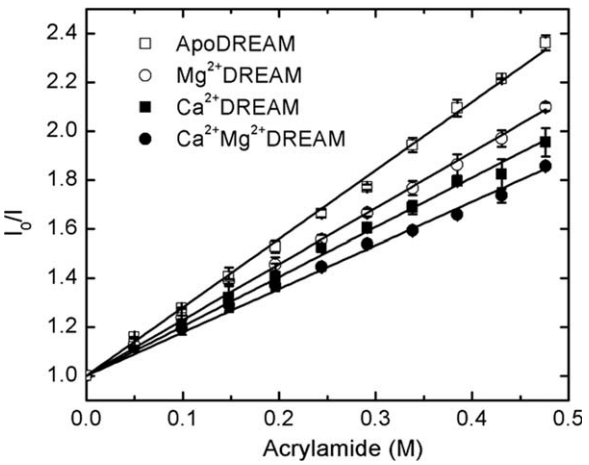

Figure 2. Stern-Volmer plot for acrylamide quenching of DREAM in the absence/presence of Ca^{2+} and Mg^{2+}. Error bar represents standard deviations of three independent measurements.

Table I. *Emission Decay Parameters for DREAM Using a Continuous Gaussian Distribution and a Discreet Component*

	τ_1 (ns)	w_1 (ns)	f_1	α_1	τ_2 (ns)	f_2	α_2	$<\tau>$ (ns)	χ^2
apoDREAM	3.6	2.0	0.77	0.88	7.5	0.23	0.12	4.5	1.7
Mg^{2+}DREAM	3.4	1.8	0.75	0.87	7.5	0.25	0.13	4.4	2.0
Ca^{2+}DREAM	1.8	0.8	0.44	0.78	7.4	0.56	0.22	4.8	1.7
$Ca^{2+}Mg^{2+}$DREAM	1.8	0.9	0.48	0.80	7.6	0.52	0.20	4.8	1.0

A constant standard error of 0.2° for the phase angle and 0.004 for modulation ratio was used. τ_1 is the mean decay time of the Gaussian distribution with a width of distribution w_1. τ_2 is the lifetime of the discrete single exponential term. The average lifetime $<\tau>$ was calculated using Eqs. (S1) and (S2) in Supporting Information section. α_1 and α_2 are normalized pre-exponential decay and f_1 and f_2 are exponential decay fractions.

Mg^{2+} DREAM and increases to 0.20 in Ca^{2+} bound forms of DREAM.

DREAM stability

The impact of Ca^{2+}/Mg^{2+} binding to EF-hands on the protein stability was characterized by monitoring the CD signal at 220 nm as a function of increasing GuHCl concentration. The unfolding curves shown in Figure 4 clearly indicate the presence of an partially folded intermediate at GuHCl concentrations between 4.0 and 5.0*M*. The experimental data were analyzed using a three-state model according to Eq. (4) and the recovered thermodynamic parameters (ΔG°, m, and C_m) are summarized in Table II. Ca^{2+} association to DREAM increases the stability of the native state compared with the unfolded state by ~4 kcal mol^{-1}, whereas the contribution of Mg^{2+} to DREAM stability is significantly smaller. Interestingly, Ca^{2+} binding to EF-hands increases the stability of the native state with respect to the partially unfolded intermediate state by ~2 kcal mol^{-1} in the presence of Mg^{2+}, whereas the stability of the intermediate state with respect to the unfolded state is increased in both Ca^{2+}DREAM and $Ca^{2+}Mg^{2+}$DREAM by ~2 kcal mol^{-1}. The shallow folding transition between the native and partially unfolded intermediate state points to a low energy barrier between the native and intermediate state for apo, Mg^{2+}, and Ca^{2+}DREAM. The native state is more strongly stabilized with respect to the intermediate state in $Ca^{2+}Mg^{2+}$DREAM, as evident from the steep transition between the folded and partially folded intermediate state.

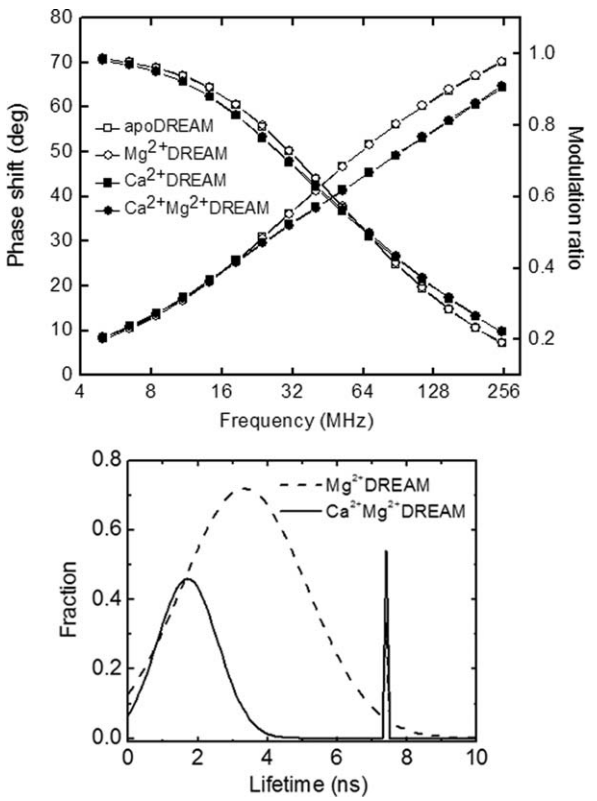

Figure 3. Top: Frequency-domain intensity decay of 40 μ*M* apo-DREAM (open squares), Mg^{2+}DREAM (open circles), Ca^{2+}DREAM (closed squares), and $Mg^{2+}Ca^{2+}$DREAM (closed circles). The solid lines represent the data fitting using a Gaussian distribution model and single exponential decay model. Note that the experimental data for apo-DREAM and Mg^{2+}DREAM are nearly identical, and likewise for the data for Ca^{2+}DREAM and $Ca^{2+}Mg^{2+}$DREAM. Bottom: Fluorescence lifetime analysis for Mg^{2+}DREAM and $Ca^{2+}Mg^{2+}$DREAM using a continuous Gaussian distribution and a discreet single exponential decay component.

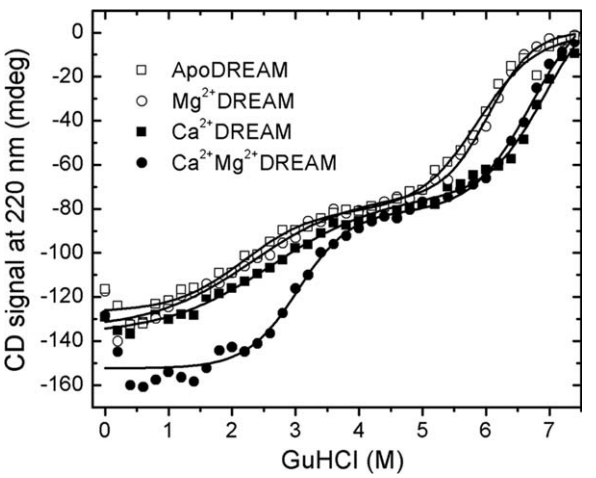

Figure 4. Representative equilibrium unfolding traces of DREAM as determined by the CD signal at 220 nm. The experimental data were fit using Eq. (4) and the thermodynamic parameters are reported in Table II.

Table II. *Thermodynamic Parameters for GuHCl-Induced Denaturation of DREAM in the Absence/Presence of Ca^{2+} and Mg^{2+}*

	$\Delta G_{N\rightarrow I}$ (kcal mol^{-1})	$m_{N\rightarrow I}$ (kcal M^{-1} mol^{-1})	$C_{N\rightarrow I}$ (M)	$\Delta G_{I\rightarrow U}$ (kcal mol^{-1})	$m_{I\rightarrow U}$ (kcal M^{-1} mol^{-1})	$C_{I\rightarrow U}$ (M)	$\Delta G_{N\rightarrow U}$ (kcal mol^{-1})
ApoDREAM	1.6 ± 0.1	0.8 ± 0.1	2.0	7.7 ± 0.8	1.3 ± 0.1	5.9	9.3 ± 0.8
Mg^{2+}DREAM	1.7 ± 0.2	0.8 ± 0.1	2.1	8.4 ± 0.9	1.4 ± 0.2	6.0	10.1 ± 0.9
Ca^{2+}DREAM	1.6 ± 0.3	0.6 ± 0.1	2.0	11.3 ± 0.1	1.7 ± 0.1	6.5	12.9 ± 0.3
$Ca^{2+}Mg^{2+}$DREAM	3.8 ± 0.4	1.2 ± 0.2	3.2	10.5 ± 1.2	1.6 ± 0.2	6.5	14.3 ± 1.3

The thermodynamic parameters were calculated using Eq. (4) where N, I, and U correspond to the native state, intermediate state, and unfolded state, respectively. ΔG is the standard free energy for the transition, m is the dependence of the free energy on the denaturant concentration, and $C_{N\rightarrow I}$ and $C_{N\rightarrow U}$ represent for denaturant concentration of half unfold from native to intermediate state and from intermediate state to unfolded state, respectively. $G_{N\rightarrow U}$ represents the overall unfolding free energy from native to unfolded state. Errors were determined from standard deviations of at least three independent measurements.

Molecular dynamics studies

Molecular dynamics simulations provide a complementary approach to monitor structural transitions in DREAM. The root mean square fluctuation (RMSF) of C_α atoms can be used to probe fluctuations of individual residues with respect to the average structure in the apo- and Ca^{2+} bound form of DREAM. The RMSF profile for a 40 ns time window is shown in Figure 5. The overall profiles are similar for apo and Ca^{2+} bound DREAM. Ca^{2+} association to EF-hand 3 and EF-hand 4 reduces the fluctuations of the Ca^{2+} binding loop in EF-hand 3 (residues 174–183), and to a smaller extent reduces the fluctuations in the binding loop of EF-hand 4 (residues 222–231). The flexibility of the long loop connecting α-helix 7 to α-helix 8 (residues 198–211) remains high in the Ca^{2+} bound form of the protein, in agreement with NMR results that show increased structural deviations in this region.[22] Interestingly, the C-terminal loop (residues 242–244) connecting α-helix 9 and α-helix10 in the C-terminal domain exhibits high flexibility in the Ca^{2+} bound structure. As expected, smaller changes in protein flexibility due to Ca^{2+} binding to DREAM are observed for the N-terminal domain of the protein.

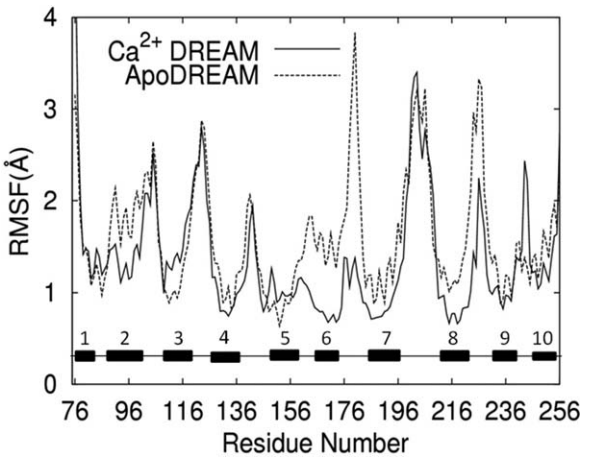

Figure 5. Root-mean-square fluctuations (RMSF) of the Cα backbone in apoDREAM and Ca^{2+}DREAM.

The superposition of MD simulations structures of apo-DREAM and Ca^{2+}DREAM monomers (Fig. 6) shows high structural similarity. Detailed inspection of these structures reveals that the N-terminal domain containing the nonfunctional EF-hand 1 and EF-hand 2 does not show significant structural differences between the apo- and Ca^{2+} bound forms apart from α-helix 2, which moves away from α-helix 5 in the Ca^{2+} bound protein. A larger structural reorganization is observed for the C-terminal domain and includes repositioning of the α-helices within the individual EF-hand binding sites. Interestingly, the entering and exiting helices of the EF-hand 3 undergo a minor reorientation in the calcium bound state with respect to the apo-state, whereas Ca^{2+} association to EF-hand 4 is accompanied by the clear transition of the α-helices from a perpendicular to a parallel orientation (Fig. 6). Also, the C-terminal helix (α-helix 10) moves away from α-helix 6 in the Ca^{2+} bound protein.

Discussion

Previous studies have demonstrated that Ca^{2+} association to the EF-hand 3 and EF-hand 4 in the C-terminal domain of DREAM leads to the dissociation of the apo-DREAM tetramer into dimers which decreases DREAM affinity for intracellular partners,[26] as well as DREAM monomer affinity for small hydrophobic molecules.[25] However, the detailed molecular mechanism of how Ca^{2+} association to the C-terminal domain EF-hands modulates the conformation of the DREAM monomer and the impact of Ca^{2+}/Mg^{2+} association on DREAM affinity for intracellular partners remains elusive. Tryptophan emission has been widely used as a sensitive probe of structural transitions in proteins including protein folding, Ca^{2+}/Mg^{2+} association to proteins and protein-protein interactions. In the DREAM structure (residues 65–256), the single Trp residue that is located at the interface between the N- and C-terminal domains provides a unique tool for characterization of Ca^{2+}/Mg^{2+} triggered conformational transitions in DREAM.

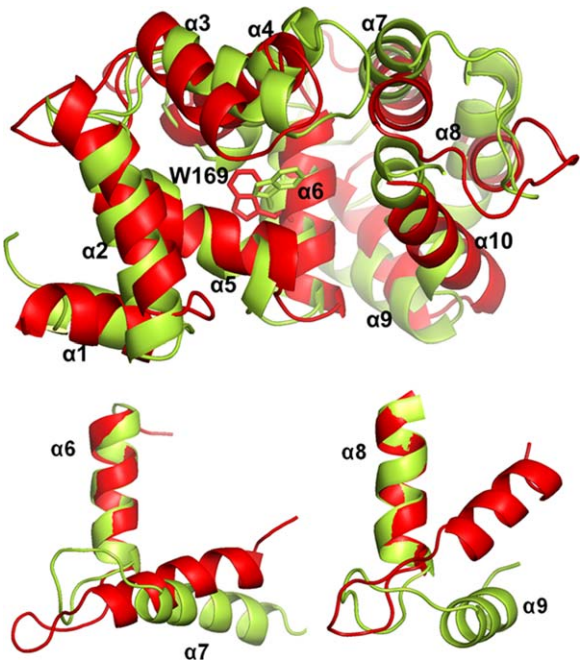

Figure 6. Top: Overlaid MD simulations structures of apo-DREAM (in red) and Ca^{2+} bound DREAM (in yellow). Alpha-helices 1 to 10 in DREAM are labeled by α1 to α10, respectively. EF-hand 1 is composed of α2 and α3, EF-hand 2 composed of α4 and α5, EF-hand 3 composed of α6 and α7, EF-hand 4 composed of α8 and α9. The position of the Trp169 residue is shown with sticks. Bottom: Ca^{2+} triggered reorganization of the EF-hand 3 (left) and EF-hand 4 (right).

Impact of Ca^{2+} binding on conformational dynamics of DREAM

Steady-state emission data of Trp169 indicate that Ca^{2+} association to EF-hand 3 and EF-hand 4 triggers the reorganization of the interface between EF-hand 2 and EF-hand 3 with the Trp side chain being located in a less polar environment in the Ca^{2+} bound form. This is further supported by the emission quenching and fluorescence lifetime data. The smaller bimolecular quenching rate constant observed for Ca^{2+}- and $Ca^{2+}Mg^{2+}$DREAM is consistent with a reduced solvent accessibility to the Trp residue due to tertiary structure alterations and/or decreased conformational flexibility in the Ca^{2+} bound form of DREAM.

The decrease in the structural flexibility is supported by the Trp lifetime data (Fig. 3). The major fraction of the Trp169 emission decay can be described using a continuous Gaussian distribution model centered at 3.5 ns for apo- and Mg^{2+} DREAM and 1.7 ns for Ca^{2+}DREAM and $Ca^{2+}Mg^{2+}$DREAM. The minor fraction (~10% in apo-DREAM and 20% in Mg^{2+} and/or Ca^{2+} bound DREAM) exhibits a discrete single exponential decay with lifetime of ~7.5 ns. The full width at half maximum value of the lifetime distribution parameter, *w*, was found to be 2.0 ns for apo- and Mg^{2+}DREAM and ~0.9 ns for Ca^{2+} bound DREAM. The observed decrease in the *w* value suggests that Ca^{2+} binding to EF-hands reduces the distribution of conformational microstates and/or modulates the dynamics of the interconversion between individual substates in DREAM.[27,28] Several mechanisms were proposed to explain the observed heterogeneity of the Trp lifetime in single Trp proteins including the presence of Trp side chain rotamers, quenching by water molecules, electron transfer to the peptide carbonyl group, excited state electron or proton transfer and intersystem crossing.[29–31] Interestingly, an overlay of the 15 lowest energy structures of Ca^{2+} bound DREAM determined by NMR spectroscopy[22] and the structure of the DREAM C-terminal domain (residues 161–256)[23] displays the presence of a single Trp rotamer (t rotamer) in the DREAM structure. However, as shown in Figure 7, a transition from the t to g+ rotamer of Trp169 sidechain is observed during molecular dynamic simulations, which support the idea that the bimodal distribution could arise from two rotameric orientations of Trp169 with the side chain of the g+ rotamer being more solvent exposed (see below). Inspection of the DREAM and DREAM C-terminal domain structures (PDB entry 2JUL and 2E6W, respectively) reveals four charged amino acid residues located within 6 Å of the Trp169 indole ring that may serve as efficient

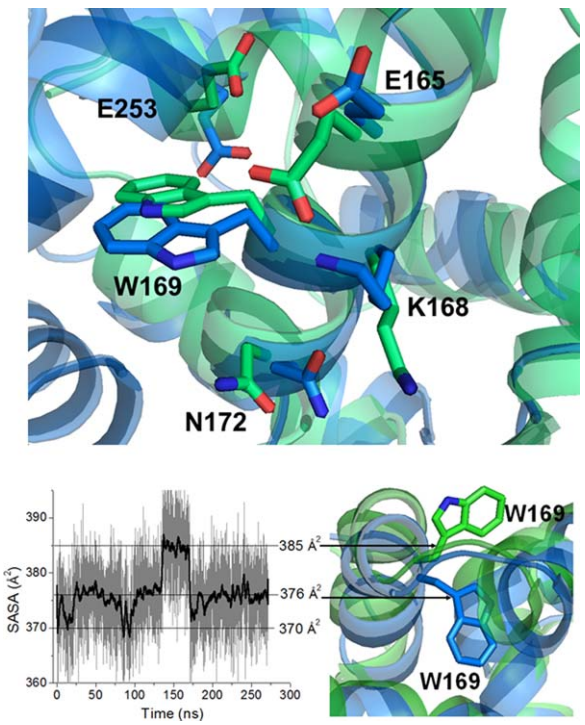

Figure 7. Top: charged and polar amino acid residues surrounding Trp169 in the structure of DREAM (PBD entry 2JUL, shown in blue) and C-terminal domain of DREAM (PBD entry 2E6W, shown in green). Bottom: Left: SASA of Trp169 in DREAM during 270 ns of the MD trajectory. Right: Partially buried (in blue) and solvent exposed (in green) orientation of Trp169 side chain in DREAM structure.

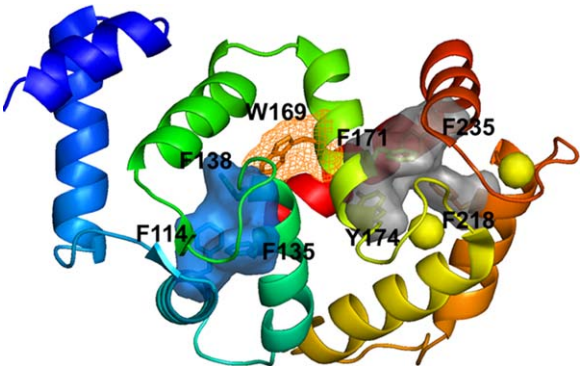

Figure 8. The aromatic clusters identified in DREAM C-terminus (grad solid surface) and N-terminus (blue solid surface). EF-hand 1 in DREAM is shown in cyan, EF-hand 2 in green, EF-hand 3 in yellow, EF-hand 4 in orange, Trp169 in wireframe surface, and calcium ions shown in yellow spheres.

quenchers for the t rotamer. Glu165, Lys168, and Asn172 are located on the same α-helix as Trp169, whereas Glu253 is found at the end of α-helix 10 (Fig. 7).In addition, the side chains of these residues are disordered in the NMR structures, which likely contribute to the observed heterogeneity of the Trp emission decay. In the absence of the NMR structure of apo-DREAM, it is difficult to pinpoint the origin of the slower Trp decay in apo- and Mg^{2+}DREAM. However, we speculate that the re-positioning of α-helix 10 upon Ca^{2+} binding brings the Glu253 side-chain closer to the Trp169 indole ring resulting in more efficient Trp emission quenching. Indeed, α-helix 10 was found to be flexible in the structure of KChIP1 as it moves away from α-helix 8 in the KChIP1:Kv4 channel T1 domain complex.[32] Also, the reorientation of the α-helix 10 was associated with increased affinity of Ca^{2+} bound DREAM for arachidonic acid and small hydrophobic molecules.[25]

The second Trp decay component is characterized by an unusually long lifetime of ~7.5 ns. It is unlikely that the presence of the second lifetime reflects other oligomerization forms of DREAM (monomer/tetramer in the case of Ca^{2+} free DREAM and monomer/dimer in the case of Ca^{2+} bound protein) since two comparable lifetimes were found for the C-terminal DREAM construct (residues 161–256) in the apo form which does not form a tetramer or dimer in solution (manuscript in preparation). On the other hand, a similar lifetime of 7.3 ns was detected in the multitryptophan protein beta-glycosidase from *Sulfolobus solfataricus,* and was associated with a rigid cluster of eight Trp residues.[33] However, the NMR structure (Fig. 7, top) and RMSF from MD simulations (Fig. 5) are not consistent with the presence of a rigid hydrophobic cluster surrounding Trp in DREAM. On the other hand, a single Trp residue in the calcium binding protein annexin was reported to exhibit two distinct lifetimes of 2.0 ns and 7.0 ns when annexin is associated to lipid vesicles.[34] The 7.0 ns decay was attributed to the Trp side-chain located in a more polar environment, at the interface between the protein surface and the lipid membrane.[34]

Thus, to further explore the dynamic behavior of the Trp side chain, a 250 ns molecular dynamics simulation was analyzed and the solvent accessible surface area (SASA) plot for Trp169 is shown in Figure 7. The Trp side chain samples three major conformations with distinct SASA values. Two conformations are characterized by SASA values of 376 $Å^2$ and 370 $Å^2$, respectively, and can be attributed to the partially buried Trp side-chain within the interface between the C- and N-terminal domains of DREAM. The additional conformation with a SASA of 385 $Å^2$ corresponds to the solvent exposed indole ring (Fig. 7). The binding site for the LDAO molecule on the DREAM surface is not known. The detergent molecule may bind into the hydrophobic cleft between the N- and C-terminal domain in a similar way as a myristoyl group binds to apo-recoverin, and thus the interactions between the Trp169 indole ring and the polar head of the LDAO molecule bound to DREAM can contribute to a 7.5 ns Trp decay and the red-shifted emission spectra of DREAM samples prepared in the presence of LDAO. Furthermore, Liao *et al.*[35] have shown that the C-terminal domain of KChIP1 is required for KChIP1 association to phospholipid vesicles and the formation of KChIP1—phospholipid vesicle complexes alters the protein structure. Taking into account a high sequence and structural homology of the C-terminal domain among the members of the KChIP subfamily, it is likely that DREAM forms similar complexes with phospholipid vesicles. Indeed, one can speculate that the DREAM conformation that is characterized by the 7.5 ns Trp lifetime reflects the conformation of DREAM associated with lipid vesicles or membranes.

DREAM stability increases in the presence of Ca^{2+}/Mg^{2+}

Association of Mg^{2+} and/or Ca^{2+} to DREAM EF-hands increases the stability of the protein, although to different extent. The unfolding data (Fig. 4) show that DREAM unfolds through a partially unfolded intermediate state that is populated at ~4.5*M* GuHCl in the case of apo- and Mg^{2+} DREAM and at ~5.0*M* GuHCl for Ca^{2+}- and $Ca^{2+}Mg^{2+}$DREAM. Further increase in the GuHCl concentration promotes protein destabilization towards the unfolded state. Unlike small, single domain proteins that fold with two-state kinetics without populating intermediate state, multidomain proteins commonly exhibit unfolding intermediates. Furthermore, protein stability and folding is modified by the presence of higher order clusters of aromatic

residues.[36,37] Such residues are usually highly conserved and their substitution often leads to the destabilization of protein structure. We have identified two aromatic hydrophobic cores in the DREAM structure (Fig. 8) that (i) are formed by residues conserved among NCS members, (ii) have a relative solvent accessibility smaller than 10%,[38] and (iii) groups side chains that are within a distance of 4.5 Å[39] of each other. One hydrophobic core is formed by an aromatic tetramer of Phe171, Tyr174, Phe218, and Phe235 and is found at the C-terminal domain (Fig. 8). All these residues are in a helical structural motif. The cluster formation brings together α-helices 6, 8, and, 9 which may stabilize the C-terminal domain. The second hydrophobic core was found within the N-terminal domain and is a trimer of phenylalanine residues (Phe114, Phe135, and Phe138) that are found in α-helices 3 and 4. Analogously to the C terminal domain, the interactions between these residues increase the stability of the N-terminal domain. In addition, Trp169 from the C-terminal domain interacts with Phe138 from the N-terminal domain and such inter-domain interactions may contribute to DREAM stability.

Considering that the Ca^{2+} association to EF-hand 3 and EF-hand 4 increases the stability of the partially unfolded intermediate with respect to the unfolded protein, we propose that α-helices 6, 8, and 9 form a stable hydrophobic core that unfolds during the intermediate between the transition and unfolded states. The N-terminal domain that lacks more extended hydrophobic core(s) may be less stable than the C-terminal domain and thus may be destabilized during the initial unfolding transition. This is further supported by the fact that the stability of the N-terminal domain is increased by the Mg^{2+} association to EF- hand 2, which is located in the N-terminal domain. Thus the unfolding data suggest that the N-terminal domain unfolds during the first transition whereas the C-terminal domain is destabilized at increased denaturant concentration. An analogous unfolding mechanism was reported previously for another member of the NCS family, neuronal calcium sensor 1 (NCS-1).[40–42] That study reported that the folding mechanism and protein stability of NCS-1 are altered by the presence of Ca^{2+} and Mg^{2+} ions as well as by the protein myristoylation at the N-terminus. Nonmyristoylated NCS1 unfolds through a three step mechanism with an overall stability of $\Delta G_{N\rightarrow U} = 12.9 \pm 0.7$ kcal mol^{-1} for apo-NCS1, and $\Delta G_{N\rightarrow U} = 14.5 \pm 1.6$ kcal mol^{-1} for holo-NCS1. These values are comparable to those determined here for apo- and Ca^{2+} bound DREAM. These results indicate a similar folding mechanism for NCS1 and DREAM, and possibly other members of the NCS family. This is further supported by a kinetic study of folding mechanisms using optical tweezers.[41] The authors have reported that the folding of the C-terminal domain precedes the folding of the N-terminal domain, and that the C-terminal domain is stabilized by aromatic interactions between α-helix 9, α-helix 8 and α-helix 6.

Material and Methods

Protein isolation and purification

The coding sequence of truncated mouse DREAM (residues 65–256) inserted into the expression vector, pReceiver B-31, with T7 promoter was purchased from GeneCopoeia. The expression vector was transformed into *Escherichia coli* BL21 (DE3) competent cells (Stratagene) and the cells were grown in 1 L of LB medium with 100 μg/mL ampicillin at 37°C until the optical density reached 0.5 at 600 nm. Expression of the recombinant protein was induced by adding 0.5 m*M* IPTG. The cells were grown overnight at 37°C and then harvested by centrifugation (8000 rpm at 4°). Protein isolation and purification were performed as described previously.[22] The purity of the protein was verified by SDS-page electrophoresis and the protein concentration was determined based on the absorbance at 280 nm ($\varepsilon_{280\ nm} = 19{,}000M^{-1}$ cm^{-1}). Absorption spectra were recorded using a single beam UV-vis spectrometer (Cary 50, Varian). To prepare Ca^{2+} and $Ca^{2+}Mg^{2+}$ bound DREAM samples, $CaCl_2$ or $MgCl_2$ solutions was added to protein samples to a final concentration of 1 m*M* Ca^{2+} and/or 5 m*M* Mg^{2+}. Apo and Mg^{2+}DREAM samples were prepared by adding 1 m*M* EDTA and 1 m*M* EGTA with 5 m*M* $MgCl_2$ to protein solutions, respectively.

Steady-state fluorescence measurements

Steady-state emission spectra were measured using a PC1 fluorimeter (ISS, Champaign, IL). For steady-state emission measurements, 40 μ*M* DREAM in 20 m*M* Tris buffer pH 7.4, 1 m*M* DTT, and 10 m*M* *N*,*N*-dimethyldodecylamine *N*-oxide (LDAO) was placed in a 0.2 x 1.0 cm quartz cell and emission spectra were recorded using 295 nm excitation. The spectra were corrected for the inner filter effect and the quantum yield for Trp emission was calculated as described using tryptophan as a standard ($\Phi = 0.13$).[43]

Fluorescence quenching

Quenching studies were performed by measuring fluorescence emission intensity in the range from 300 nm to 450 nm using an excitation wavelength of 295 nm, after addition of small aliquots of freshly prepared 10*M* acrylamide solution following 5 min incubation. The decrease in the emission intensity at 340 nm and 335 nm for the Ca^{2+} free and Ca^{2+} bound form of DREAM, respectively, was corrected for the inner filter effect. The data were analyzed using the Stern-Volmer equation:

$$\frac{I_0}{I} = 1 + K_{SV}[Q] \quad (1)$$

where I_0 and I correspond to the fluorescence intensities in the absence and presence of quencher, respectively. K_{SV} is the Stern-Volmer quenching constant, and $[Q]$ is the quencher concentration.

Time-resolved fluorescence measurements

The frequency domain fluorescence lifetime measurements were performed on a ChronoFD fluorometer (ISS, IL-Champaign). The output of a 280 nm light emitting diode was frequency modulated in the range between 5 and 250 MHz. The emission was collected through a 320 nm long pass filter (Andover Inc.) and detected using a PMT (R928, Hamamatsu). The fluorescence decay data were analyzed using a combination of a single Gaussian distribution and a single discrete component according to Eqs. (2) and (3).[44]

$$I(t) = a_1 \int_0^\infty \rho(\tau)^{-t/\tau} d\tau + a_2 \exp(-t/\tau_2) \quad (2)$$

and

$$\rho(\tau) = \frac{1}{w_1\sqrt{2\pi}} \exp\left[-\frac{1}{2}\left(\frac{\tau-\tau_1}{w_1}\right)^2\right] \quad (3)$$

where a_1 and a_2 represent the amplitude of each term in Eq. (2) and τ_1 is the mean decay time of the Gaussian distribution with a width of distribution w_1. τ_2 is the lifetime of the discrete single exponential term. The data analysis was performed using the Globals for Spectroscopy Software (Laboratory of Fluorescence Dynamics, University of California, Irvine). The reference compound used in lifetime measurements was 2,5-diphenyloxazole (PPO) in ethanol (τ = 1.40 ns).[45]

DREAM stability studies

GuHCl induced protein unfolding was monitored by measuring the CD spectra as a function of increasing GuHCl concentration. Samples for CD measurements were prepared by solubilizing 40 μ*M* DREAM in 20 m*M* Tris-HCl, 1 m*M* DTT, 10 m*M* LDAO, pH 7.4, and incubated in the presence of GuHCl for 30 min before CD measurements. The CD spectra were recorded using a Jasco J-810 CD-spectrometer at 16°C. DREAM unfolding traces were analyzed as a two-step process involving an intermediate state:

$$N \leftrightarrow I \leftrightarrow U \quad (4)$$

where N corresponds to the native state, I to the partially unfolded intermediate state, and U to the unfolded state. The unfolding curves were fit using the following equation:[46,47]

$$Y(\text{GuHCl}) = \frac{Y_N + Y_I \exp\left[\frac{-(\Delta G^\circ_I - m_I[D])}{RT}\right] + Y_U \exp\left[\frac{-(\Delta G^\circ_I - m_I[D] + \Delta G^\circ_U - m_U[D])}{RT}\right]}{1 + \exp\left[\frac{-(\Delta G^\circ_I - m_I[D])}{RT}\right] + \exp\left[\frac{-(\Delta G^\circ_I - m_I[D] + \Delta G^\circ_U - m_U[D])}{RT}\right]} \quad (5)$$

where Y(GuHCl) is the CD signal at 220 nm, ΔG is the standard free energy for the unfolding, m is the dependence of the free energy on the denaturant concentration, T is the temperature (T = 289 K), $[D]$ is the concentration of GuHCl, and R is the ideal gas constant, R = 8.314 JK^{-1} mol^{-1}. The parameters Y_N, Y_I, and Y_U represent the 220 nm CD signal of each molecular species at zero GuHCl concentration.

Molecular dynamics simulations

Time series molecular dynamics (MD) trajectories were obtained from explicit solvent, all-atom simulations using the molecular dynamics simulation package NAMD[48] with the CHARMM27 force field.[49] The initial NMR structure of the DREAM protein was obtained from the Protein Data Bank (PDB code 2JUL). The protein was solvated using the VMD package[50] with a box cutoff set to 10 Å. This resulted in a simulation box of dimensions 81.5 × 68.6 × 58.1 Å. The solvated system was electrically neutralized by adding 12 Na^+ ions randomly in the bulk water using the VMD autoionize plugin. The particle mesh Ewald method[51] was used to treat long-range interactions with a 12 Å nonbonded cutoff. Energy minimization (50,000 steps) was performed using the conjugate gradient and line search algorithm. The system was then heated for 90 ps with a linear gradient of 20 K/6 ps from 20 to 300 K. At 300 K, the system was equilibrated for 910 ps with a 2 fs integration time step in the NVT (constant number, volume, and temperature) ensemble. Langevin dynamics was used to maintain the temperature at 300 K. The production run was 67 ns using NVT dynamics with 2 fs time steps. The same

procedure was used to setup another system of a DREAM protein without calcium ions for simulating the apo-state of the protein. An additional 270 ns simulation was conducted for calcium bound DREAM using AMBER03 force fields with a 10 Å PME cut off and 1.25 fs integration time, all other parameters being identical.

Summary

Despite the low impact of Mg^{2+} association with EF-hand 2 on the DREAM tertiary structure, the presence of Mg^{2+} stabilizes the native state with respect to a partially unfolded state. The Trp lifetime data indicates that DREAM can adopt an additional conformation with a long Trp lifetime of 7.5 ns that may reflect conformations of DREAM populated in the presence of lipid membranes and vesicles. The results show that DREAM unfolding is a complex process that occurs through an partially unfolded, intermediate state. The Ca^{2+} association to EF-hand 3 and 4 stabilizes the partially unfolded state with respect to the unfolded state whereas the association of the Mg^{2+} increases the stability of the native state only in the presence of Ca^{2+}. These results suggest that the intracellular fluctuations in Ca^{2+} and Mg^{2+} concentrations control the global conformation and stability of DREAM and likely regulate its interactions with intracellular partners.

References

1. Gifford JL, Walsh MP, Vogel HJ (2007) Structures and metal-ion-binding properties of the Ca2+-binding helix–loop–helix EF-hand motifs. Biochem J 405:199–221.
2. Bhattacharya S, Bunick CG, Chazin WJ (2004) Target selectivity in EF-hand calcium binding proteins. Biochim Biophys Acta 1742:69–79.
3. Chazin WJ (2011) Relating form and function of EF-hand calcium binding proteins. Acc Chem Res 44:171–179.
4. Burgoyne RD, Weiss JL (2001) The neuronal calcium sensor family of Ca2+-binding proteins. Biochem J 353:1–12.
5. Ames JB, Lim S (2012) Molecular structure and target recognition of neuronal calcium sensor proteins. Biochim Biophys Acta 1820:1205–1213.
6. Burgoyne RD (2007) Neuronal calcium sensor proteins: generating diversity in neuronal Ca2+ signalling. Nat Rev Neurosci 8:182–193.
7. Haynes LP, Burgoyne RD (2008) Unexpected tails of a Ca2+ sensor. Nat Chem Biol 4:90–91.
8. Ames JB, Lim S, Ikura M (2012) Molecular structure and target recognition of neuronal calcium sensor proteins. Front Mol Neurosci 5:10.
9. An WF, Bowlby MR, Betty M, Cao J, Ling H, Mendoza G, Hinson JW, Mattsson KI, Strassle BW, Trimmers JS, Rhodes KJ (2000) Modulation of A-type potassium channels by a family of calcium sensors. Nature 403: 553–556.
10. Schwenk J, Zolles G, Kandias NG, Neubauer I, Kalbacher H, Covarrubias M, Fakler B, Bentrop D (2008) NMR analysis of KChIP4a reveals structural basis for control of surface expression of Kv4 channel complexes. J Biol Chem 283:18937–18946.
11. Jerng HH, Pfaffinger PJ, Covarrubias M (2004) Molecular physiology and modulation of somatodendritic A-type potassium channels. Mol Cell Neurosci 27:343–369.
12. Zhou W, Qian Y, Kunjilwar K, Pfaffinger PJ, Choe S (2004) Structural insights into the functional interaction of KChIP1 with Shal-Type K+ channels. Neuron 41:573–586.
13. Ramachandran PL, Craig TA, Atanasova EA, Cui G, Owen BA, Bergen HR, 3rd, Mer G, Kumar R (2012) The potassium channel interacting protein 3 (DREAM/KChIP3) heterodimerizes with and regulates calmodulin function. J Biol Chem 287:39439–39448.
14. Carrion AM, Link WA, Ledo F, Mellstrom B, Naranjo JR (1999) DREAM is a Ca2+-regulated transcriptional repressor. Nature 398:80–84.
15. Jo DG, Chang JW, Hong HS, Mook-Jung I, Jung YK (2003) Contribution of presenilin/gamma-secretase to calsenilin-mediated apoptosis. Biochem Biophys Res Commun 305:62–66.
16. Jo DG, Jang J, Kim BJ, Lundkvist J, Jung YK (2005) Overexpression of calsenilin enhances gamma-secretase activity. Neurosci Lett 378:59–64.
17. Jang C, Choi J-K, Na Y-J, Jang B, Wasco W, Buxbaum JD, Kim Y-S, Choi E-K (2011) Calsenilin regulates presenilin 1/γ-secretase-mediated N-cadherin ϵ-cleavage and β-catenin signaling. FASEB J 25:4174–4183.
18. Buxbaum JD (2004) A role for calsenilin and related proteins in multiple aspects of neuronal function. Biochem Biophys Res Commun 322:1140–1144.
19. Buxbaum JD, Choi EK, Luo Y, Lilliehook C, Crowley AC, Merriam DE, Wasco W (1998) Calsenilin: a calcium-binding protein that interacts with the presenilins and regulates the levels of a presenilin fragment. Nat Med 4:1177–1181.
20. Ledo F, Kremer L, Mellström B, Naranjo JR (2002) Ca2+-dependent block of CREB–CBP transcription by repressor DREAM. EMBO J 21:4583–4592.
21. Ledo F, Carrión AM, Link WA, Mellström B, Naranjo JR (2000) DREAM-αCREM interaction via leucine-charged domains derepresses downstream regulatory element-dependent transcription. Mol Cell Biol 20: 9120–9126.
22. Lusin JD, Vanarotti M, Dace A, Li C, Valiveti A, Ames JB (2008) NMR structure of DREAM: Implications for Ca2+-dependent DNA binding and protein dimerization. Biochemistry 47:2252–2264.
23. Yu L, Sun C, Mendoza R, Wang J, Matayoshi ED, Hebert E, Pereda-Lopez A, Hajduk PJ, Olejniczak ET (2007) Solution structure and calcium-binding properties of EF-hands 3 and 4 of calsenilin. Protein Sci 16:2502–2509.
24. Osawa M, Tong KI, Lilliehook C, Wasco W, Buxbaum JD, Cheng HY, Penninger JM, Ikura M, Ames JB (2001) Calcium-regulated DNA binding and oligomerization of the neuronal calcium-sensing protein, calsenilin/DREAM/KChIP3. J Biol Chem 276:41005–41013.
25. Gonzalez WG, Miksovska J (2014) Application of ANS fluorescent probes to identify hydrophobic sites on the surface of DREAM. Biochim Biophys Acta 1844:1472–1480.
26. Osawa M, Dace A, Tong KI, Valiveti A, Ikura M, Ames JB (2005) Mg2+ and Ca2+ differentially regulate DNA binding and dimerization of DREAM. J Biol Chem 280:18008–18014.
27. Bódis E, Raics K, Nyitrai M, Majer Z, Lukács A (2013) Fluorescence lifetime distributions report on protein destabilisation in quenching experiments. J Photochem Photobiol B 129:108–114.

28. Alcala JR, Gratton E, Prendergast FG (1987) Interpretation of fluorescence decays in proteins using continuous lifetime distributions. Biophys J 51:925–936.
29. Szabo AG, Rayner DM (1980) Fluorescence decay of tryptophan conformers in aqueous solution. J Am Chem Soc 102:554–563.
30. Moncrieffe MC, Juranić N, Kemple MD, Potter JD, Macura S, Prendergast FG (2000) Structure-fluorescence correlations in a single tryptophan mutant of carp parvalbumin: solution structure, backbone and side-chain dynamics. J Mol Biol 297:147–163.
31. Ross JA, Jameson DM (2008) Time-resolved methods in biophysics. 8. Frequency domain fluorometry: applications to intrinsic protein fluorescence. Photochem Photobiol Sci 7:1301–1312.
32. Wang H, Yan Y, Liu Q, Huang Y, Shen Y, Chen L, Chen Y, Yang Q, Hao Q, Wang K, et al. (2007) Structural basis for modulation of Kv4 K+ channels by auxiliary KChIP subunits. Nat Neurosci 10:32–39.
33. Bismuto E, Nucci R, Rossi M, Irace G (1999) Structural and dynamic aspects of β-glycosidase from mesophilic and thermophilic bacteria by multitryptophanyl emission decay studies. Proteins 35:163–172.
34. Follenius-Wund A, Piémont E, Freyssinet J-M, Gérard D, Pigault C (1997) Conformational adaptation of annexin V upon binding to liposomes: a time-resolved fluorescence study. Biochem Biophys Res Commun 234:111–116.
35. Liao Y, Chen K, Chang L (2009) Functional role of EF-hands 3 and 4 in membrane-binding of KChIP1. J Biosci 34:203–211.
36. Song Z, Zheng X, Yang B (2013) Conformational stability of CopC and roles of residues Tyr79 and Trp83. Protein Sci 22:1519–1530.
37. Burley S, Petsko G (1985) Aromatic-aromatic interaction: a mechanism of protein structure stabilization. Science 229:23–28.
38. Rost B, Sander C (1994) Conservation and prediction of solvent accessibility in protein families. Proteins 20: 216–226.
39. Arunachalam J, Gautham N (2008) Hydrophobic clusters in protein structures. Proteins 71:2012–2025.
40. Aravind P, Chandra K, Reddy PP, Jeromin A, Chary KVR, Sharma Y (2008) Regulatory and structural EF-hand motifs of neuronal calcium sensor-1: Mg2+ modulates Ca2+ binding, Ca2+-induced conformational changes, and equilibrium unfolding transitions. J Mol Biol 376:1100–1115.
41. Heidarsson P, Otazo M, Bellucci L, Mossa A, Imparato A, Paci E, Corni S, Di Felice R, Kragelund B, Cecconi C (2013) Single-molecule folding mechanism of an EF-hand neuronal calcium sensor. Structure 21:1812–1821.
42. Muralidhar D, Jobby MK, Krishnan K, Annapurna V, Chary KVR, Jeromin A, Sharma Y (2005) Equilibrium unfolding of neuronal calcium sensor-1: N-terminal myristoylation influences unfolding and reduces protein stiffening in the presence of calcium. J Biol Chem 280:15569–15578.
43. Lakowicz JR (2010) Principles of fluorescence spectroscopy. New York: Springer.
44. Togashi D, Ryder A, O'Shaughnessy D (2010) Monitoring local unfolding of bovine serum albumin during denaturation using steady-state and time-resolved fluorescence spectroscopy. J Fluor 20:441–452.
45. Boens N, Qin W, Basarić N, Hofkens J, Ameloot M, Pouget J, Lefévre J-P, Valeur B, Gratton E, vandeVen M, Silva N, Engelborghs Y, Willaert K, Sillen A, Rumbles G, Phillips D, Visser A, van Hoek A, Lakowicz J, Malak H, Gryczynski I, Szabo A, Krajcarski D, Tamai N, Miura A (2007) Fluorescence lifetime standards for time and frequency domain fluorescence spectroscopy. Analyt Chem 79:2137–2149.
46. Hung H-C, Chen Y-H, Liu G-Y, Lee H-J, Chang G-G (2003) Equilibrium protein folding-unfolding process involving multiple intermediates. Bull Math Biol 65: 553–570.
47. Santoro MM, Bolen DW (1988) Unfolding free energy changes determined by the linear extrapolation method. 1. Unfolding of phenylmethanesulfonyl .alpha.-chymotrypsin using different denaturants. Biochemistry 27:8063–8068.
48. Phillips JC, Braun R, Wang W, Gumbart J, Tajkhorshid E, Villa E, Chipot C, Skeel RD, Kalé L, Schulten K (2005) Scalable molecular dynamics with NAMD. J Comput Chem 26:1781–1802.
49. Brooks BR, Bruccoleri RE, Olafson BD, States DJ, Swaminathan S, Karplus M (1983) CHARMM: a program for macromolecular energy, minimization, and dynamics calculations. J Comput Chem 4:187–217.
50. Humphrey W, Dalke A, Schulten K (1996) VMD: visual molecular dynamics. J Mol Graph 14:33–38, 27–38.
51. Essmann U, Perera L, Berkowitz ML, Darden T, Lee H, et al. (1995) A smooth particle mesh Ewald method. J Chem Phys 103:8577–8593.